DOI: 10.13009/EUCASS2017-114

Control of Incident Shock Induced Separation at Mach 3.5 using an Array of Steady Micro-Jet Actuators

Manisankar Chidambaranathan, E. Rathakrishnan** and S B Verma**
**Scientist*
Experimental Aerodynamics Division, CSIR-NAL, Bangalore, India
***Professor*
Department of Aerospace Engineering, IIT-Kanpur, India

Abstract
Experiments were conducted to understand the effectiveness of an active flow control device in modifying the separation characteristics of an incident shock induced separation in a Mach *3.5* flow. The objective of the study was to understand the modifications brought in to the separation process by (i) varying the pitch and skew angles of the micro-jet axis and, (ii) by varying the spanwise spacing and control pressure of the jets. Of all the configurations tested, the most effective device is seen to be the micro-jet array with 90^o pitch and skew angles which significantly modifies the overall separation characteristics.

1. Introduction

The losses associated with the interaction between the strong incident shock wave and the growing boundary layer often leads to deviation from the mission objectives of the vehicle. It is expected to occur in intake region, fins, wings etc. If the interaction is considered to be strong enough [1] they forms a massive separation bubble which causes unstart phenomena in intake, localised peak heating on the surface, structural damage due to unsteady loads. Figure. 1 shows typical incident shock wave boundary layer interaction occurring in a flat plate. When the incident shock wave (C_1) strength is considered strong enough the interaction introduces a large adverse pressure gradient to the growing boundary layer, which in turn leads to lifting of the boundary layer [2] from the solid wall surface which form a shear layer. As the supersonic freestream flow over the shear layer, series of compression waves are generated which coalesce to form a separation shock (C_2). The point where the separation shock meets the incident shock give rise to two more shocks, transmitted shock (C_3) and reflected shock (C_4). The transmitted shock on encountering the shear layer reflect back as an expansion fan which pushes the shear layer towards the wall surface creating series of compression waves which coalesce to form reattachment shock wave. It is observed in earlier studies [3] that the separation shock is found to be highly unsteady possessing low frequency and high amplitude oscillation. Lot of work has been done in past to identify the cause for such low frequency pulsation, based on which different types of mechanism have been proposed in the literature. Some of them point to the influence of the upstream incoming boundary layer flow structures [4,5] and others point the mass imbalance between the separation region and reattachment region cause breathing effect [6,7] which in turn is responsible for the low frequency oscillation.

The shockwave and boundary layer interaction is a naturally occurring phenomena which cannot be avoided, therefore the flow control techniques like bleeding, active/passive control are considered to be effective in modifying the separation characteristics[8]. Independent trade studies by Lockheed-Martin [9] shows that the usage bleed will reduce the mission range by 20% and further studies by Boeing phantoms work [10] shows increase in gross total overweight by 10%. Therefore the flow control techniques like active method (micro-jet, plasma, etc.) or passive devices like ramp vane, rectangular vane, Anderson type, etc are generally used. These active/passive device are designed to generate micro-vortical structures that are embedded inside the boundary layer which helps to energise the boundary layer by mixing between low momentum and high momentum flow inside the boundary layer. The passive devices are considered advantageous when it comes for ruggedness and lower wave drag. At the same time the passive devices introduce larger viscous drag, added to this they suits only for certain design conditions. On the other hand the active device like micro-jet enjoy the benefit of having lower viscous drag; flexible to implement over large area in the model surface. The major challenge in implementing the active devices as flow control comes in the form of requirement for additional mechanism and payload needed to supply the energy, further they introduce significant amount of wave drag if not properly designed and distributed.

DOI: 10.13009/EUCASS2017-114

The objective of the study was to understand the modifications brought in to the overall separation process i) by varying the pitch ($\beta = 90°, 45°$) and skew ($\alpha = 0°, 135°$) angles of the micro-jet axis (*MJVG1-2*) ii) by reducing the spanwise spacing of MJs (*MJVG3*) and, iii) by varying the micro-jet injection pressure (P_{oj}).

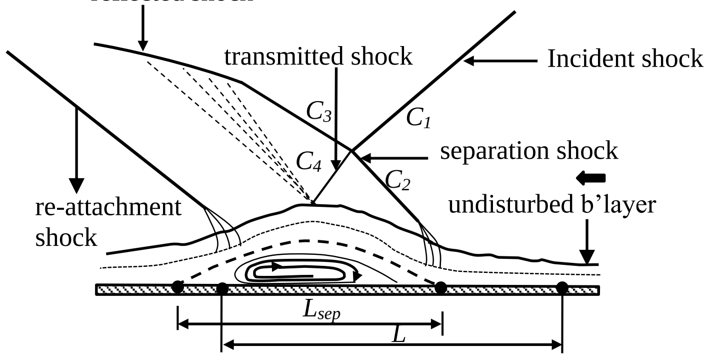

Figure. 1 Schematic of the incident shockwave boundary layer interaction

2. Experimental setup and model details

2.1 Wind tunnel and free stream flow conditions

Experiments were carried out in the tri-sonic wind tunnel facility in National Aerospace Laboratories (NAL). It is a blow down type wind tunnel with test section size of 0.46 m × 0.3 m. To avoid the tunnel wall boundary layer associated noise, the base plate of the model where the SWBLI (Shock Wave Boundary-layer Interaction) occurs was elevated to the tunnel centerline using the supporting strut as in Figure 2. The free stream Mach number was 3.5 ±0.02 for which the free stream velocity was 647 m/s . The tunnel stagnation pressure (P_o) and total temperature (T_o) was maintained at 682.58 kPa ± 2% and 298 K ± 0.4% respectively. The Reynolds number per unit length (Re/L) corresponding to the free-stream flow condition was 38.1×10^6 m^{-1}.

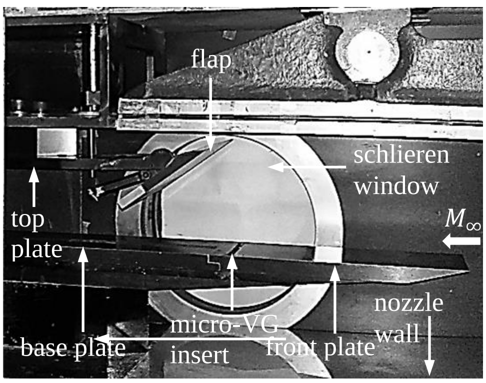

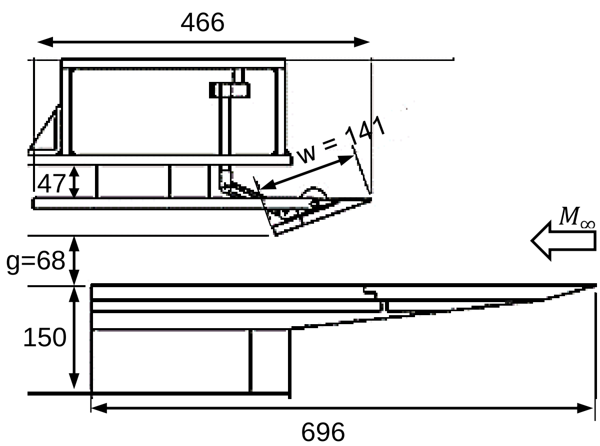

Figure. 2 Experimental setup details

2.2 Model details

The experimental setup used for this study is schematically shown in figure.2. A wedge with a flow turning angle of 22° was used to generate an oblique shock wave with an angle of 39.4° which was made to interact with the growing boundary layer on the base plate as shown in figure.2. For the given flow turning angle and experimental setup the g/w was 0.5. The base plate of the model was 696 mm and 110 mm wide as in figure. 3. The Reynolds number based on the base plate model was 26.5×10^6. There was no fence attached on the sides of the base plate model to allow for schlieren flow visualization of the interaction region. To make sure the flow was turbulent, a trip of 4mm length made using carborundum particle of size 60 grit was located at 17mm from the leading edge as in figure. 3.

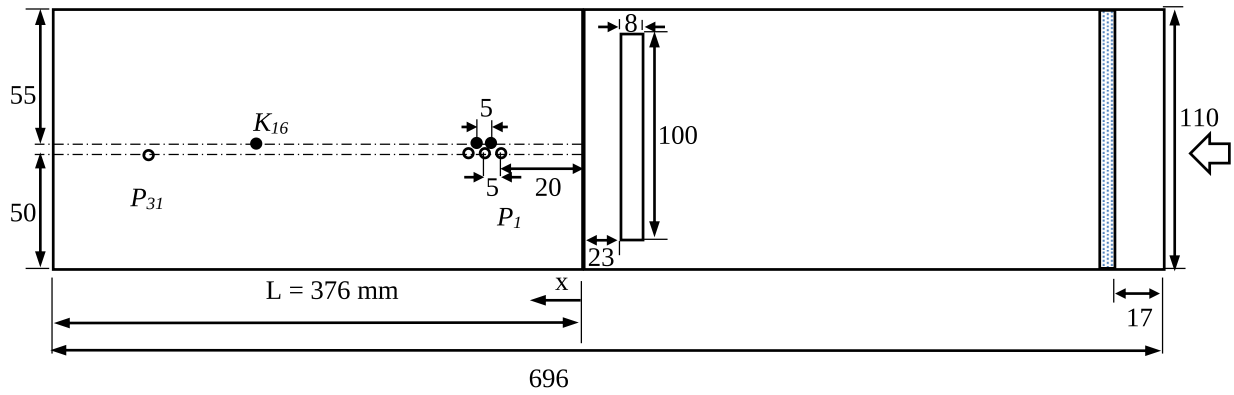

Figure. 3 Flat plate model details

2.3 Micro-jet model details

The flow control devices used for this study were in the form of an array of micro-jets. The device was placed 14δ ahead of the separation point (where δ is the boundary layer thickness at the point where the impinging shock is supposed to meet the wall if the boundary layer is considered absent, δ=6.4 mm). Based on the micro-jet exit axis inclination (pitch angle, β and skew angle, α) two different configurations *MJVG1-2* were fabricated as shown in figure. 4a-b. The reduction in the spanwise spacing was studied using *MJVG3* with the α=0° and β = 90° as in figure. 4c. For *MJVG1-2* there were 14 micro-jet holes with 0.5mm diameter and 5mm pitch between each hole and 27 holes with 2.5mm pitch for *MJVG3* as shown in figure. 4c. Each configuration has an inbuilt stagnation chamber that ensures uniformity of the jet momentum issuing from all the openings. A nitrogen cylinder of tank pressure 13.8 MPa was connected via a manifold to the in-built stagnation chamber of the micro-jet device. The micro-jet stagnation pressure line was monitored using digital pressure indicator (with 200psid range). The micro-jet flow properties like micro-jet pressure ratio (MPR), momentum flux ratio (J), momentum coefficient (Cμ) are given in table.1.

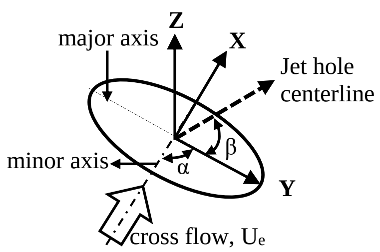

a) micro-jet model coordinate details

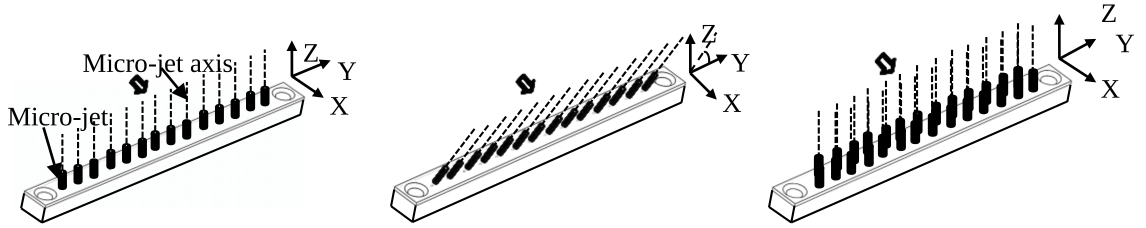

b) MJVG1 (α=90°; β=90°) c) MJVG2 (α=135°; β=45°) d) MJVG3 (α=90°; β=90°)

Figure. 4 Micro-jet model details

DOI: 10.13009/EUCASS2017-114

2.4 Data acquisition details

The stream wise wall pressure distribution was obtained on the base plate of the model using both the mean and unsteady transducers. The mean pressure ports are distributed as in figure. 3 indicated by P_1 to P_{22}. These mean pressure ports were connected to an Electronic Pressure Scanner (ESP) of model number ESP-16HD. The in-situ method was adopted for calibrating the scanner for which a Druck calibrator of model DPI-610 was utilized. The analog signal from the ESP scanner was acquired using 8 channel signal conditioner module from National Instruments of model SCXI-1520. The acquired analog signal was digitized using 16-bit Analog to Digital card (ADC) NI 6036 consisting of 16 channels with maximum sampling rate of 200 kS/s. For the current experimental work, the data was sampled at the rate of 1000 S/s with 1000 Samples per port location leading to sampling time interval of 1s. The fluctuations in the wall pressure and the associated unsteadiness was acquired using 16 piezo-resistive transducers of model Kulite XCQ-093 M-screen transducer. The location of the transducers on the base plate in the stream wise direction is marked as K_1 to K_{16} as in figure. 3. In this study 200 records containing 4096 data points of data were acquired for each channel at a sampling frequency of 50 kHz making a total of 819200 data points per channel per run. To extract the frequency component from the unsteady signal, a narrow band Fast Fourier Transform (*FFT*) with frequency resolution of 12.2 Hz was initially carried out on each record containing 4096 points which was finally averaged for all the 200 records.

Table 1: micro-jet flow details

P_{oj}, in kPa	**MPR**	**J**	**C_μ**
125	0.2	0.63	1.34E-09
180	0.28	0.91	1.92E-09
277.5	0.42	1.39	2.94E-09
551	0.84	2.78	5.87E-09

3. Results and Discussion

3.1 Schlieren flow visualisation

Figure. 5 a-d shows the schlieren image for fixed flow turning angle of $\theta = 22°$ with and without the flow control device. It can be visualized in the no-control case that there is no major perturbation in the flow until it approaches the separation point. Although few weak waves are visible at the junction of baseplate and front plate, the wave angle was measured to be around *17°* which is approximately equal to the Mach angle(μ*=16.6°*) for M_∞=3.5 flow. The flow visualization image for the no control case as in figure .5a shows the presence of incident shock, separation shock, reflected shock and transmitted shock wave as discussed earlier in the sub-section 1. The separation angle was measured from the schlieren image which is approximately $\varphi=35°$. The shear layer formed as a result of the separation of boundary layer from the wall surface is seen as dark patch for both control and no-control cases. As the flow control was applied with $P_{oj}=125$ *kPa* the separation point is observed to be shifted slightly downstream approximately by 0.5δ (where δ is the boundary layer thickness at the point of separation, $\delta=6.4mm$) as in figure. 5b. The separation shock angle was observed to be not altered ($\varphi=35°$) with the introduction of the flow control. For the rise in injection pressure to $P_{oj}=277.5$ *kPa* the separation point is pushed downstream to approximately *1δ*, the shift in separation point is observed till the injection pressure reaches $P_{oj} \leq 277.5$ *kPa*. Beyond $P_{oj} > 277.5$ *kPa* the separation is moved upstream which may be the result of jet to jet iteration occurring between the micro-jet in span wise direction as discussed in detail in literature [11].

DOI: 10.13009/EUCASS2017-114

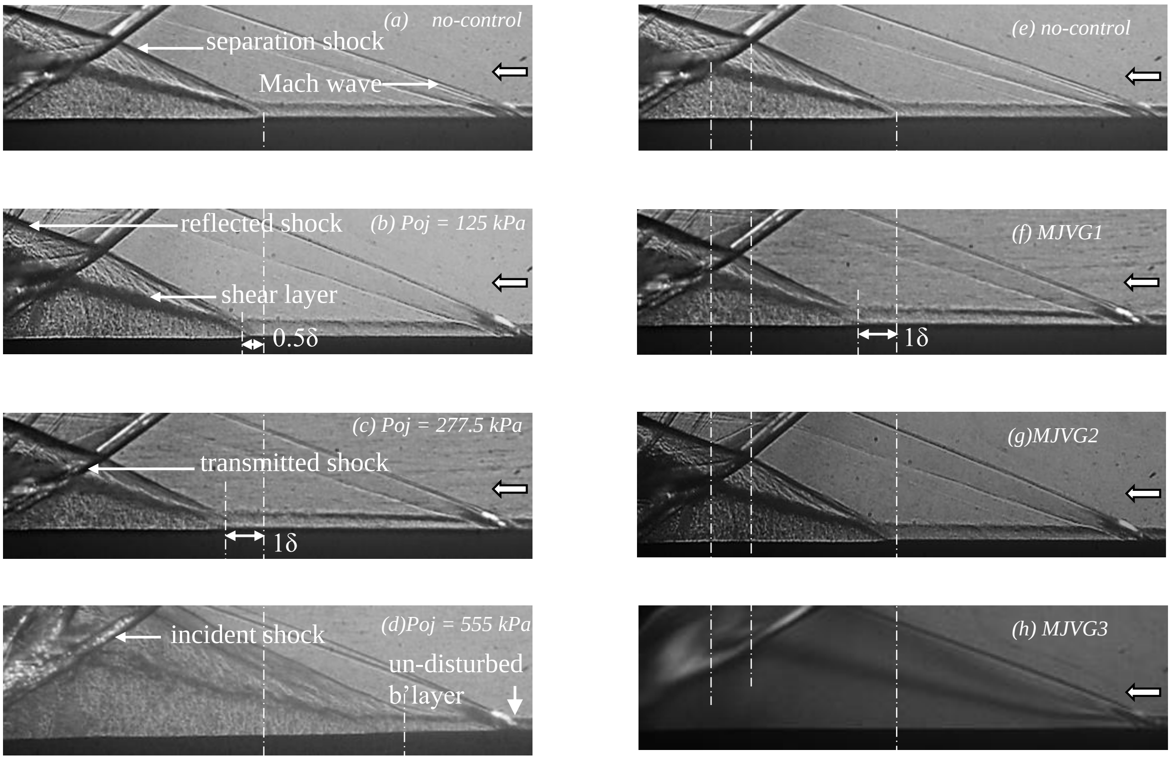

Figure. 5 Schlieren visualisation i) for (a-d) the injection pressure was varied from *no-control* to P_{oj}=555 kPa ; ii) for (e-h) the different control device *MJVG1-3* with constant P_{oj} of 277.5 kPa

Figure. 5(e-h) shows the schlieren image with different flow control device for the constant injection pressure of P_{oj}*=277.5 kPa* with the fixed flow turning angle of $\theta = 22°$. As the flow control *MJVG1* is introduced the flow visualization as in figure. 5f shows the separation was pushed by approximately *1δ* distance downstream. The point where the transmitted shock meets the shear layer appears to occur at the same location which ensures that the separation shock angle remain unaltered as discussed above, with the introduction of flow control. On the other hand for the flow control device *MJVG2*, there is no major shift in the separation point location relative to the no-control case. This shows that the effect of pitching and skewing the micro-jet axis has larger impact in modifying the separation characteristics. For the reduction in the span wise spacing of flow control device *MJVG3* there is no major shift in the separation point location relative to the no-control case. The above result signifies that in-order to have an effective flow control device the span wise spacing, pitch angle and skew angle has to be properly designed for a particular application.

3.2 Mean pressure and *rms* value

Figure. 6a shows the mean pressure distribution for the flow control device without control and with flow control *MJVG1*. For no-control case, the pressure value remain almost constant till it approach *x/L* of 0.13, after which there is steep rise in pressure indicating the starting of intermittent interaction region. The point where tangent drawn along the pressure rise deviates marks the onset of the physical separation point [12, 13], which is seen at *x/L*=0.17 for the no-control. The steep pressure rise is followed by the constant pressure line which indicates the beginning of the separation bubble region. As the flow control *MJVG1* is introduced the interaction region in the mean pressure distribution show some variation, with a shift in its location to *x/L* of 0.14 for P_{oj}=180 *kPa*. With further increase of injection pressure P_{oj}=277.5 *kPa*, the separation point shift further to *x/L*=0.15 which is about 13% change relative to the no-control case. However as the injection pressure is increased beyond, P_{oj} > *277.5 kPa* the separation point slowly started to move upstream which may be the result of jet to jet interaction along the span wise direction.

DOI: 10.13009/EUCASS2017-114

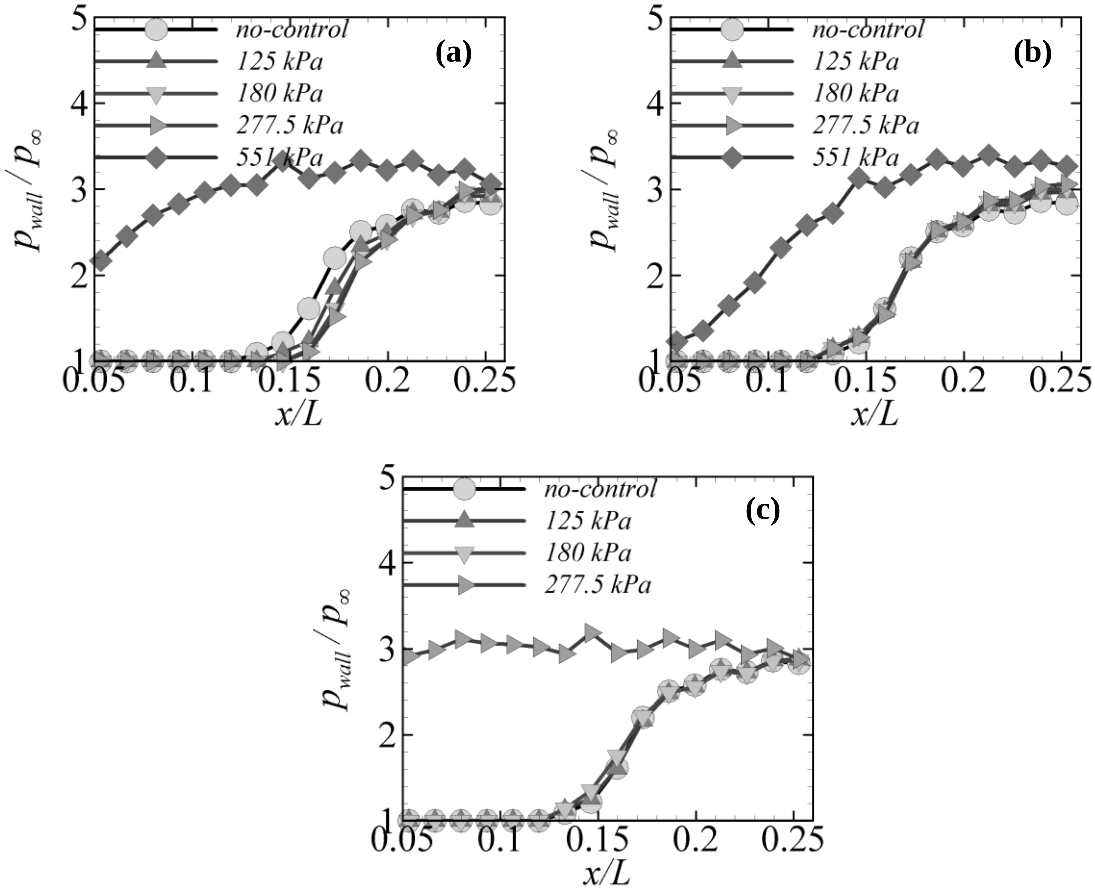

Figure. 6 Mean pressure distribution for a) *MJVG1* b) *MJVG2* c) *MJVG3*

In case of flow control *MJVG2* as seen in figure. 6b the mean pressure data at the separation point is invariant at *x/L*= 0.13 till the injection pressure of P_{oj}=277.5 *kPa*, beyond this injection pressure the separation pressure starts to move in upstream direction. Similar to *MJVG2* the mean pressure values for the *MJVG3* also shows an overlap of the values as in figure. 6c till P_{oj}=180 *kPa*, beyond this value the separation moves upstream which is much early compared to other *MJVGs* and is attributed to closer jet spacing which results in flow blockage and hence a condition similar to intake unstart.

The non-dimensionalised *rms* variation with and without flow control device is shown in figure. 7a. The *rms* value remain almost constant till it approach the beginning of the interaction region *x/L*=0.13, where the *rms* start the rise and achieve a peak in value after which it start to fall drastically indicating the end of intermittent oscillation region. With the increase in the injection pressure the *rms* rise is shifted downstream, which is in line with the mean pressure distribution shift observed earlier. But the peak *rms* value remain unaltered even with the application of the flow control, indicating that the flow control device only modifies the separation point location without altering the associated unsteadiness. In the case of *MJVG2* as in figure. 7b the *rms* value almost overlaps with that of the no-control, which is expected as the mean pressure data and schlieren flow visualisation shows no change in separation point shift relative to no-control. The *MJVG3* device also shown similar *rms* trend as seen for *MJVG2* as in figure. 7c

DOI: 10.13009/EUCASS2017-114

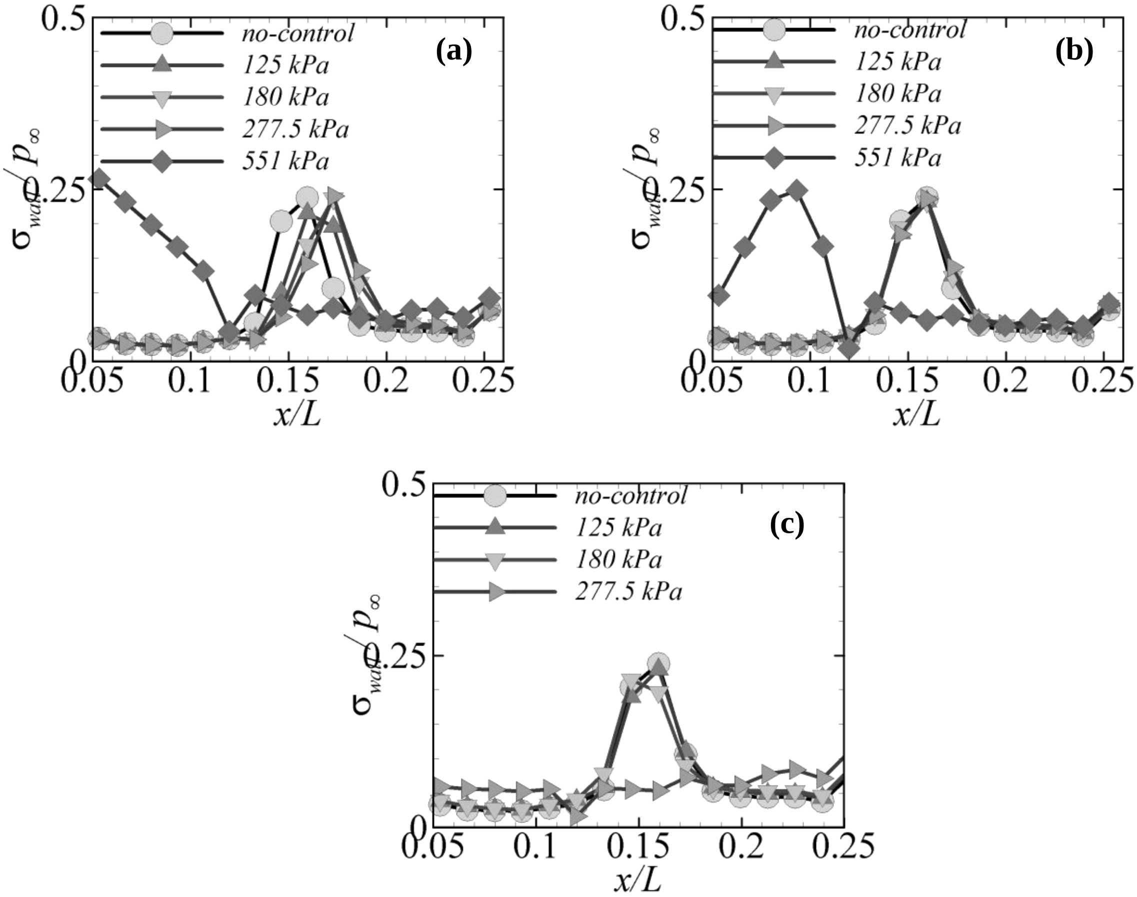

Figure. 7 *rms* distribution for a) *MJVG1* b) *MJVG2* c) *MJVG3*

3.3 Intermittency and spectral distribution

Figure. 8a shows the real time wall pressure signal for no-control at the interaction region for two different locations *x/L*= 0.14, $\gamma = 0.17$ and at *x/L*=0.16, $\gamma = 0.69$ for the flow turning angle (θ) of 22°. The shock passage causes a steep rise and fall in the pressure values at certain time intervals as in figures. 8a, 8c. The plot shows a low and high pressure values occurring at random interval. The time at which the low pressure value occurs corresponds to un-disturbed upstream boundary layer pressure values which the transducer was exposed and high correspond to behind the shock values.

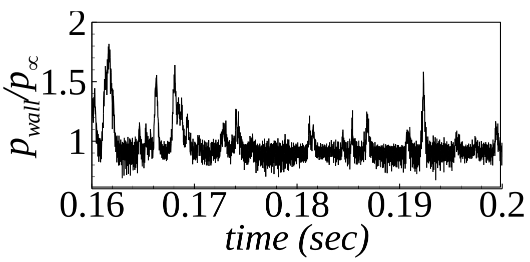

a) real time wall pressure at γ=0.17

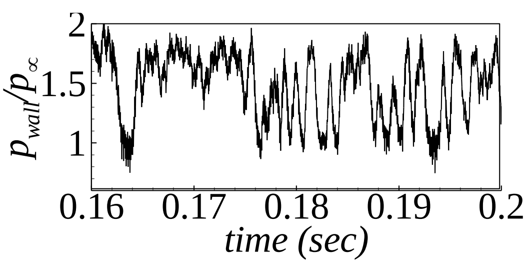

c) real time wall pressure at γ=0.69

DOI: 10.13009/EUCASS2017-114

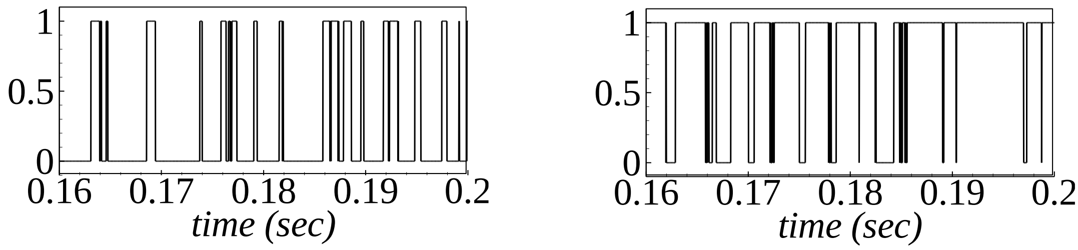

b) box car signal at γ=0.17   d) boxcar signal at γ=0.69

Figure. 8 Real time pressure signal and box-car signal at γ of 0.17 and 0.69

In order to capture the variation in the signal (low and high values) a conditional sampling technique [14] was adopted. This technique modifies the real time wall pressure signal into a box-car function, where the algorithm count the number of shock crossings for a given transducer location. The two threshold limits $T_1=P_w+3\sigma_{pw}$ and $T_2=P_w+6\sigma_{pw}$ discussed by Brusnaik and Dolling [14] were set to avoid the counting the turbulent fluctuations as shock crossing. The real time wall pressure signal was converted into the series of 0’s (time when the pressure value corresponds to incoming boundary layer value) and 1’s (downstream of the shock) using the two threshold. Figure. 8b shows the box-car signal at the two x/L = 0.14 where the signal most of time spend in zeros and figure. 8d corresponds to x/L = 0.16 where it spends more time in 1’s.

The intermittency factor can be defined as the percentage of the time the shock spends upstream of the transducer location to that of the total time. The percentage of time spent upstream of the transducer is obtained by counting the number of 1’s in the condition sampled signal.
Intermittency factor (γ) is given by [15]

$$\gamma = \frac{\text{time}\left[P_w > \left(\bar{P}_w + 6\sigma_{bl}\right)\right]}{\text{total time}}$$

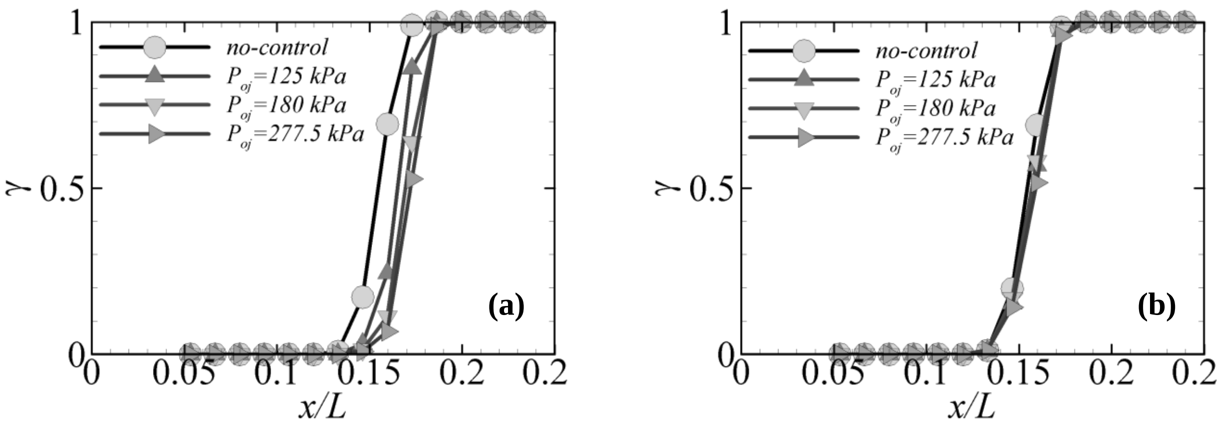

Figure. 9 Intermittency distribution γ=0.69 for a) *MJVG1* b) *MJVG2*

Figure. 9a shows the intermittency distribution for the *MJVG1* with different injection pressures, the intermittency value is zero in the incoming boundary layer region. On approaching the intermittent oscillation region x/L=0.13(for no-control) the intermittency slowly start to rise up when it reaches the x/L=0.16 the intermittency value reaches peak value of 1. Based on the intermittent values it is possible to mark a boundary for extent of the unsteady interaction region, where the upstream boundary is marked when γ attains 1% of the value, on reaching γ of 90% of the value downstream boundary starts. The measured distance from the upstream to the downstream boundary is generally defined as the intermittent region length, L_s ($0.1\leq \gamma \geq 0.9$) [16]. For the no-control case the L_s was calculated to be 10.75 mm or 1.68δ. With the introduction of the flow control P_{oj}= 125 *kPa* the intermittent value start rise from x/L=0.14 as in figure. 9a, which follows the trend as seen earlier for the mean pressure and *rms* variations. However

DOI: 10.13009/EUCASS2017-114

the value of *Ls* = 10.75mm remain unaltered, which indicates that *MJVG1* doesn't alter the unsteadiness of shock. Further increase of P_{oj} ≥180 *kPa* shows the intermittent rise always occurs at same location of *x/L*=0.15. Figure. 9b-9c shows the intermittent value for the *MJVG2* and *MJVG3*, both the plots show complete overlap of the values with no-control, which is expected as the flow visualisation and mean pressure distribution shown no major change in the separation point location relative to the no-control case.

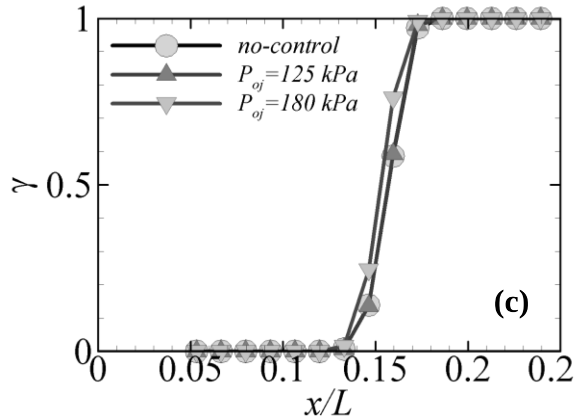

Figure. 9c Intermittency distribution γ=0.69 for *MJVG3*

The technique widely used to categorise the dynamic signal temporally is spectral analysis. To get the relative frequency content in the real time pressure signal normalized *PSD* function $G(f)\ f\ /\sigma_p{}^2$ was used for this study. The spectra usually reveals the dominant frequency in the signal occurs at low frequency (200 to 500 Hz) with high amplitude energy level of the signal. The shock frequency is usually expressed in non-dimensional form using Strouhal number $St = f_s\ L\ /U_\infty$ in which f_s is the characteristic shock oscillation frequency and L is the separation length measured between median of separation of the shock and extrapolated incident shock approximately 0.102 m for no-control case and U_∞ is the free stream velocity (647 m/s). The previous work on incident shock related interactions shows *St* to be approximately between 0.02 to 0.03 for Mach 3.5 flow for which the f_s was estimated to be around 100Hz to 500Hz.

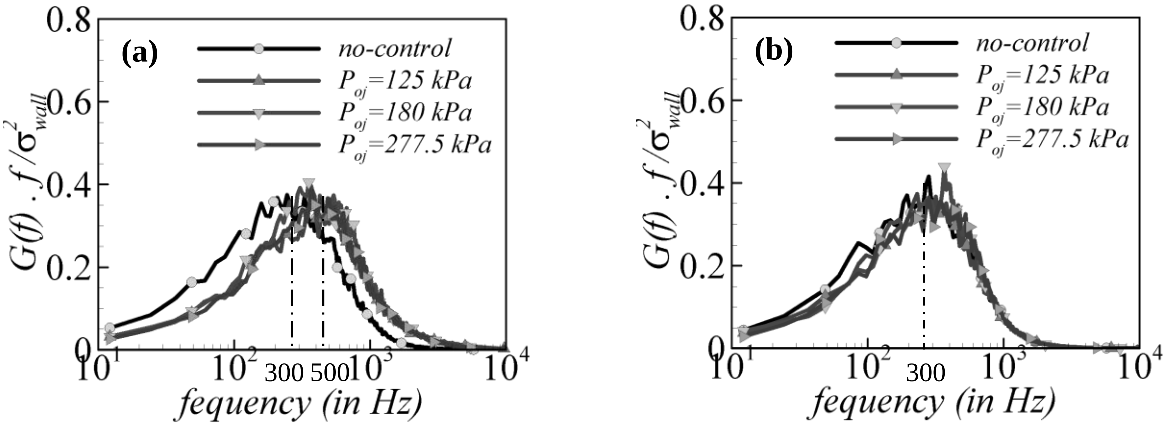

Figure. 10 Spectral distribution at γ=0.69 for a) *MJVG1* b) *MJVG2*

Figure. 10a shows the spectral plot for the *MJVG1* at $\gamma = 0.69$ with different injection pressures. For no-control the dominant frequency in the spectra was centred around 300 Hz. With the application of the flow control P_{oj}= 180 kPa the dominant frequency was shifted to the 500 Hz, which shows the flow control was successful in modifying the dominant frequency, which is one of the major objective in this work. However when the injection pressure reaches P_{oj}≥ 180 kPa the spectra shows dominant frequency still lies in 500 Hz which indicates for the given *MJVG1* design the maximum shift in the dominant frequency achievable is 500 Hz. Figure. 10b-10c shows the spectra at $\gamma = 0.69$ for *MJVG2* and *MJVG3* with different injection pressures. The dominant frequency value is centred around 300 Hz for all the injection pressure values (which is the same as no-control case), therefore it can be said that for these devices the flow control is ineffective in modifying the spectral energy in the shock oscillation frequency range.

DOI: 10.13009/EUCASS2017-114

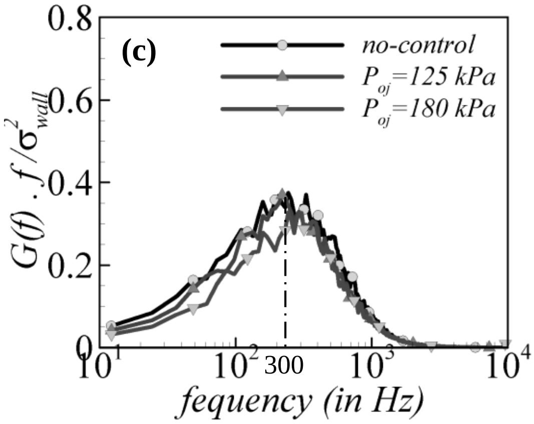

Figure.10c Spectral distribution at γ=0.69 for *MJVG3*

4. Conclusion

Experiments were carried out at M_∞=3.5 to control the separation induced by an incident shock wave and a growing turbulent boundary layer on the flat plate surface. The shock wave was generated using a wedge of flow turning angle 22° with g/w ratio of 0.5. The flat plate surface where the interaction occurred was instrumented with unsteady transducers. Schlieren flow visualisation was done using spark as the light source. The flow control used for this study was made up of an array of micro-jet holes placed at 14δ ahead of the interaction region. The micro-jet device effectiveness was studied with the variation in i) the pitch angle (β) and skew angle (α) ii) the spanwise spacing between the jets iii) with modification in the injection pressure (P_{oj}). The results from the flow visualisation shows with the introduction of flow control *MJVG1* the separation point is pushed to a maximum of 1δ for the injection pressure of P_{oj}=180 kPa. Further increase in the injection pressure resulted in movement of the separation point to upstream location, which may be due to the jet to jet interaction occurring along the spanwise direction. The change in skew angle to α =135°, *MJVG2* shows no major change in the separation point location relative to the no-control for all the injection pressures. The reduction in spanwise spacing shows the separation point is pushed to forward location even for lower injection pressures P_{oj}=277.5 kPa, which shows the jet to jet interaction play vital role in the design of the flow control device.

The mean pressure distribution shows relative to no-control for the *MJVG1* with the injection pressure of P_{oj}=277.5 kPa there is about 13.5% downstream shift in the separation shock. However beyond P_{oj} of 277.5 kPa the pressure rise is shifted upstream, which is in line with flow visualisation where the separation shock showed upstream movement at higher injection pressures. For the case of *MJVG2* the mean pressure data shows an overlap of the values between control and the no-control case. In the case of *MJVG3* the pressure rise shows a shift in the forward direction even at lower injection pressure P_{oj} =277.5 kPa. The rms variation for the *MJVG1* shows a shift in the peak value rms along the stream wise location with the increase of the injection pressure. However for all the control device the peak rms value remain unaltered with the variation in the control pressures indicating that the flow control is ineffective in suppressing the unsteady nature of the separation shock. The intermittent value distribution also showed a shift in the location of the separation shock for the *MJVG1* for the variation in the injection pressure. However the intermittent length ($L_{s,no\text{-}control}$) value remain unaltered with the introduction of the control ($L_{s,control}$=10.75mm) which reiterates that the control device *MJVG1* only shifts the separation point location whereas the unsteadiness value remain unaltered relative to no-control. As expected for the *MJVG2* and *MJVG3* the intermittent value overlaps with the no-control values. The spectral analysis for *MJVG1* at the location where the γ=0.69 shows there is a shift in dominant frequency value from 300 Hz to 500 Hz which shows the effectiveness of using the flow control. On the other hand for the flow control device *MJVG2* and *MJVG3* the dominant frequency remain unaltered at 300 Hz.

The above results clearly indicate that in-order to have an effective flow control device to modify the separation characteristics the parameters like pitch angle (*β*), skew angle (*α*), span wise spacing and the injection pressures (P_{oj}) plays crucial role.

DOI: 10.13009/EUCASS2017-114

References

[1] J. E. Green, “Interactions between shock waves and turbulent boundary layers”, *Progress in Aerospace science*, Vol. 11, 235-340, (1970)

[2] Délery, Jean, "Dussauge, Jean Paul, “Some physical aspects of shock wave/boundary layer interactions. “*Shock Waves*”, 19(6), 453–468, (2009).

[3] Humble, R. A., Scarano, F., Van Oudheusden, B. W., Unsteady aspects of an incident shock wave/turbulent boundary layer interaction, “*Jounal of fluid Mechanics*”, Vol.635, pp-47-74, (2009)

[4] Beresh, P. L., Clemens, N. T., and Dolling, D. S., Relationship Between Upstream Turbulent Boundary-Layer Velocity Fluctuations and Separated Shock Unsteadiness, “*AIAA Journal*”, Vol. 40, No. 12, 2002, pp. 2412–2422.

[5] Ganapathisubramani, B., Clemens, N.T., and Dolling, D. S., Effects of Upstream on the Unsteadiness of Shock Induced Separation, “*Journal of Fluid Mechanics*”, Vol. 585, Aug. 2007, pp. 369–394

[6] Maull, D. J., Hypersonic Flow over Axially Symmetric Spiked Bodies, “*Journal of Fluid Mechanics*”, Vol. 8, No. 4, 1960, pp. 584–592.

[7] Charwat, A. F., Dewey, C. F., Roos, J. N., and Hitz, J. A., Investigation of Separated Flows, Part 2; Flowin Cavity and Heat Transfer, “*Journal of the Aerospace Sciences*”, Vol. 28, No. 7, 1961, pp. 513–527.

[8] Dolling D. S., FiftyYears of Shock-Wave/Boundary-Layer Interaction Research: What Next?, “*AIAA Journal*”, Vol. 39, No. 8, 2001, pp. 1517–1531.

[9] Pegg, R.J., Hunt, J.L., Petley, D.H., Burkardt, L., Stevens, D.R., Moses, P.L., Pinckney, S.Z., Kabis, Z.K., Spoth, K.A., Dziedzic, W.M., Kreis, R.I., Martin, J.G., Barnhart, P.J., Design of a Hypersonic Waverider-Derived Airplane, “*AIAA 1993-0401*”

[10] Loth, E, Smart Mesoflaps for Control of Shock Boundary Layer Interactions, “*AIAA Paper 2000-2476*”

[11] Verma, S. B., Manisankar, C., Shockwave/Boundary-Layer Interaction Control on a Compression Ramp Using Steady Micro Jets, “*AIAA Journal*”, 50, 2753-2764, (2012)

[12] Stark, R., Beitrag zum Verständnis der Strömungsablösung in Raketendüsen, “*Ph.D Thesis*”, Ins. fuer Aerodynamik and Gasdynamik, Univ. Stuttgart, Germany (2010).

[13] Verma, S.B., Shock unsteadiness in a thrust optimized parabolic nozzle. “*Shock Waves*”, 19(3), 193–212 (2009).

[14] Dolling, D. S., Brusniak, L., Separation shock motion in fin, cylinder, and compression ramp - Induced turbulent interactions, “*AIAA Journal*”, 27, 734-742, (1989).

[15] Dolling, D. S., Smith, D. R., Separation shock dynamics in Mach 5 turbulent interactions induced by cylinders, “*AIAA Journal*”, 27, 1698-1706, (1989).

[16] Barter, John W., Dolling, David S., Reduction of fluctuating pressure loads in shock wave turbulent boundary layer interactions, “*AIAA Journal*”, Vol. 33, 1842-1849, (1995).